Scientific Reports

https://doi.org/10.1038/s41598-026-38152-z

Article in Press

Spinal cord involvement and cardiovascular autonomic dysfunction in Parkinson's disease

Received: 24 September 2025

Accepted: 29 January 2026

Published online: 17 March 2026

Cite this article as: Chougar L., Lejeune F., Cohen-Adad J. *et al.* Spinal cord involvement and cardiovascular autonomic dysfunction in Parkinson's disease. *Sci Rep* (2026). https://doi.org/10.1038/s41598-026-38152-z

Lydia Chougar, François-Xavier Lejeune, Julien Cohen-Adad, Caroline Landelle, Mathieu Guay-Paquet, Joshua Newton, Jan Valosek, Emma Biondetti, Carna Jovanovic, Karl Wennberg, Alain Dagher, Julien Doyon, Nadya Pyatigorskaya, Sara Sambin, Graziella Mangone, Jean-Christophe Corvol, Isabelle Arnulf, Marie Vidailhet & Stéphane Lehéricy

We are providing an unedited version of this manuscript to give early access to its findings. Before final publication, the manuscript will undergo further editing. Please note there may be errors present which affect the content, and all legal disclaimers apply.

If this paper is publishing under a Transparent Peer Review model then Peer Review reports will publish with the final article.

ARTICLE IN PRESS

© The Author(s) 2026. **Open Access** This article is licensed under a Creative Commons Attribution-NonCommercial-NoDerivatives 4.0 International License, which permits any non-commercial use, sharing, distribution and reproduction in any medium or format, as long as you give appropriate credit to the original author(s) and the source, provide a link to the Creative Commons licence, and indicate if you modified the licensed material. You do not have permission under this licence to share adapted material derived from this article or parts of it. The images or other third party material in this article are included in the article's Creative Commons licence, unless indicated otherwise in a credit line to the material. If material is not included in the article's Creative Commons licence and your intended use is not permitted by statutory regulation or exceeds the permitted use, you will need to obtain permission directly from the copyright holder. To view a copy of this licence, visit http://creativecommons.org/licenses/by-nc-nd/4.0/.

ARTICLE IN PRESS

Research Article

Title: Spinal cord involvement and cardiovascular autonomic dysfunction in Parkinson's disease

Lydia Chougar,[1,2] François-Xavier Lejeune,[3] Julien Cohen-Adad,[4-7] Caroline Landelle,[2] Mathieu Guay-Paquet,[4] Joshua Newton,[4] Jan Valosek,[4,5] Emma Biondetti,[8,9] Carna Jovanovic,[10] Karl Wennberg,[2] Alain Dagher,[2] Julien Doyon,[2] Nadya Pyatigorskaya,[1] Sara Sambin,[11] Graziella Mangone,[11] Jean-Christophe Corvol,[11] Isabelle Arnulf,[11] Marie Vidailhet,[11] Stéphane Lehéricy[1]

[1] Sorbonne Université, Institut du Cerveau - Paris Brain Institute - ICM, AP-HP, CNRS, Inserm, Hôpital de la Pitié Salpêtrière, DMU DIAMENT, Department of Neuroradiology, F-75013, Paris, France, Paris, France

[2] The Neuro - Montreal Neurological Institute and Hospital, McGill University, Montreal H3A 2B4, Canada

[3] ICM, Data Analysis Core (DAC), Sorbonne Université, Institut du Cerveau - Paris Brain Institute - ICM, CNRS, Inserm, F-75013, Paris, France

[4] NeuroPoly Lab, Institute of Biomedical Engineering, Polytechnique Montreal, Montreal, Quebec, Canada

[5] Mila - Quebec AI Institute, Montreal, Quebec, Canada

[6] Functional Neuroimaging Unit, CRIUGM, University of Montreal, Montreal, Quebec, Canada

[7] Research Center, Ste-Justine Hospital University Centre, Montreal, Quebec, Canada

[8] Department of Neurosciences, Imaging, and Clinical Sciences, University 'G. D'Annunzio' of Chieti-Pescara, Chieti, Italy

[9] Institute for Advanced Biomedical Technologies, University 'G. D'Annunzio' of Chieti-Pescara, Chieti, Italy

ARTICLE IN PRESS

ARTICLE IN PRESS

[10] *Neurology Clinic, University Clinical Center of Serbia, Belgrade, Serbia*

[11] *Sorbonne Université, Institut du Cerveau - Paris Brain Institute - ICM, AP-HP, CNRS, Inserm, Hôpital de la Pitié Salpêtrière, Department of Neurology, F-75013, Paris, France, Paris, France*

Corresponding author:

Lydia Chougar MD PhD
The Neuro - Montreal Neurological Institute and Hospital, McGill University
3801 Rue University, Montreal, QC H3A 2B4, Canada
514-9295-771, lydia.chougar@mcgill.ca

ARTICLE IN PRESS

ARTICLE IN PRESS

Abstract

Background: Patients with Parkinson's disease (PD) frequently present autonomic cardiovascular dysfunction. This study investigated the involvement of autonomic centers in the upper thoracic spinal cord in cardiovascular dysfunction in patients with PD using multimodal MRI and markers of orthostatic hypotension.

Methods: We recruited 26 patients with PD, stratified based on the presence ($PD_{RBD(+)}$, n=11) or absence ($PD_{RBD(-)}$, n=15) of rapid-eye movement sleep behavior disorder (RBD), and 22 matched healthy controls (HC). Participants underwent multimodal MRI of the cervical and upper thoracic spinal cord. Quantitative metrics, including T1 relaxation times, diffusion metrics, and magnetization transfer ratio (MTR) values, were extracted from gray and white matter spinal cord regions. MRI metrics were compared across groups and examined for associations with blood pressure drops, both cross-sectionally and longitudinally, as indicators of orthostatic hypotension.

Results: No significant differences in MRI metrics were found between patients with PD and HCs, nor between PD subgroups. A multivariate analysis pooling all MRI metrics together allowed for the separation of HCs and PD subgroups. In the $PD_{RBD(+)}$ subgroup, positive correlations were found between systolic blood pressure drop and T1 relaxation times as well as mean diffusivity values at the cervicothoracic junction. Longitudinal changes in blood pressure drops were associated with MRI measurements after adjusting for baseline blood pressure, age, and sex, suggesting that these metrics may serve as potential markers of future blood pressure changes.

Conclusions: These preliminary findings suggest that spinal cord quantitative MRI measurements at the cervicothoracic junction may be associated with orthostatic hypotension in $PD_{RBD(+)}$ patients.

Keywords: Parkinson's disease, Spinal cord, Quantitative MRI, Autonomic Dysfunction, Orthostatic Hypotension.

ARTICLE IN PRESS

Introduction

Parkinson's disease (PD) is a neurodegenerative disorder that involves the autonomic nervous system,[1,2] contributing to the frequent dysautonomic symptoms observed in patients. Notably, the cardiovascular system is affected, resulting in symptoms such as neurogenic orthostatic hypotension and cardiac rhythm disturbances.[3,4] Cardiac innervation is provided by the parasympathetic and sympathetic systems. Preganglionic neurons of the parasympathetic system are located in several nuclei of the brainstem and in the sacral parasympathetic nuclei of the spinal cord segments S2 to S4. The vagus nerve, which originates in the medulla oblongata, innervates the sinoatrial and atrioventricular nodes of the heart.[5] In PD, neurodegeneration affects the dorsal motor nucleus of the vagus nerve in the medulla oblongata.[1,2] Involvement of this nucleus, as seen on multimodal magnetic resonance imaging (MRI), was shown to correlate with cardiac rhythm abnormalities during sleep.[6] On the other hand, preganglionic neurons of the sympathetic system targeting the heart are located in the intermediolateral cell column (IML) of the upper thoracic spinal cord.[7] The presence of pathological α-synuclein inclusions in the spinal cord, particularly in the IML, is almost constant in patients with PD.[2,8,9]

Furthermore, two main models of pathology propagation have been proposed based on histological evidence by Braak et al. [1] and, more recently, *in vivo* imaging studies.[10–13] In the first model, the initial pathology originates in the enteric nervous system and propagates in an ascending manner to the central nervous system via the peripheral system. In the second model, the pathology arises in the olfactory bulb or amygdala and spreads in a descending fashion.[10–13] Previous studies suggested that the ascending model may be associated with the presence of rapid-eye movement sleep behavior disorder (RBD) and characterized by early autonomic damage preceding involvement of the nigrostriatal dopaminergic system.[10–13] Conversely, the descending model has been observed in RBD-negative PD patients.[10,11,13] Although these models remains debated,[11] spinal cord damage might be more severe in patients with RBD compared to those without RBD.

Recently, MRI has been used to detect spinal cord abnormalities in diseases such as spinal-muscular amyotrophy,[14] amyotrophic lateral sclerosis [15], and spinal cord trauma.[16] Morphometry derived from T2-weighted images

ARTICLE IN PRESS

provides a measure of atrophy, diffusion imaging probes tissue microstructure by characterizing the diffusion of water molecules and can therefore inform on tissue damage, T1 relaxometry is also hypothesized to reflect microstructural tissue properties, and magnetization transfer contrast serves as a proxy for tissue myelination.[17] Taken together, these techniques appear promising for exploring spinal cord alterations in PD.

In the current study, we aimed to investigate spinal cord alterations in patients with PD in comparison with healthy controls (HC), and to assess its relationship with clinical markers of autonomic dysfunction, such as orthostatic hypotension, cross-sectionally and then longitudinally, using multimodal spinal cord MRI. We hypothesized that PD patients would exhibit structural alterations in the upper portion of the thoracic spinal cord, that these alterations would be more prominent in patients with RBD compared to those without RBD, and that such changes would be associated with cardiac autonomic dysfunction observed in PD.

ARTICLE IN PRESS

Methods and Materials

Participants

This prospective study was conducted as part of the ICEBERG study, a five-year longitudinal project aimed at identifying and validating markers to predict and monitor the progression of dopaminergic and non-dopaminergic lesions in early and prodromal PD.

Patients with PD, along with age- and sex-matched HCs, were recruited at the Paris Brain Institute (ICM) between 2020 and 2023. The diagnosis of PD was established according to the MDS clinical diagnostic criteria for PD.[3] Polysomnography was used to assess the presence or absence of rapid-eye movement sleep behavior disorder (RBD) in our sample of PD patients, who were then stratified based on the presence ($PD_{RBD\ (+)}$) or absence ($PD_{RBD\ (-)}$) of RBD.

After visual inspection of all raw images (performed by L.C.), participants were excluded in cases of poor image quality related to motion and/or significant susceptibility artifacts, marked cervical lordosis, disk protrusion compressing the spinal cord, or any spinal cord signal abnormality.

ARTICLE IN PRESS

The study was performed in accordance with the Declaration of Helsinki and was approved by the institutional ethical standard committee (CPP Paris VI/RCB: 2014-A00725-42). All participants gave written informed consent.

Clinical data

The following clinical scores were collected in PD patients at the time of MRI: disease duration, Movement Disorder Society Unified Parkinson's Disease Rating Scale (MDS-UPDRS) [18] part III, Hoehn and Yahr stage,[19] REM Sleep Behavior Disorder Screening Questionnaire (RBDSQ),[20] and SCales for Outcomes in PArkinson's disease - Autonomic Dysfunction (SCOPA-AUT) scores including the cardiovascular subscore.[21] Participants were assessed for the presence or absence of orthostatic hypotension, defined as a drop in systolic blood pressure ≥ 20 mmHg or diastolic blood pressure ≥ 10 mmHg within 3 or 5 minutes of standing compared to baseline blood pressure (defined as the mean of two measurements on the upper right arm with the participant in the supine position after 5 min of rest).[22] In addition, systolic and diastolic blood pressure drops were also recorded at baseline and five-year follow-up visits.

MRI acquisition

Spinal MRI scans were performed at either the first- or the third-year follow-up visit. Participants were scanned in the on state using a 3 Tesla Siemens PRISMA scanner (Siemens Healthcare, Erlangen, Germany) using a 32-channel posterior spine coil, an 18-channel flex body coil placed anteriorly and covering the neck area, and a 64-channel head-neck coil. The field of view covered the cervical and upper thoracic spinal cord from C2 to T5 vertebral levels, thus including the cardiovascular autonomic control centers located in the upper thoracic region. The MRI protocol comprised (see supplementary Table S1 for details about the acquisition parameters; supplementary Figure S1):

- 3D turbo spin echo T2-weighted acquisition, voxel size: 0.8-mm isotropic.
- Diffusion-weighted imaging (DWI) echo planar imaging (EPI) with cardiac gating; b-value = 1000 s/mm^2; 64 diffusion encoding directions; voxel size = 1.3 × 1.3 × 5 mm^3; three adjacent axial slabs covering the spinal cord from C2 to T5 vertebral levels.
- 3D gradient echo images acquired with (MT on) and without (MT off) magnetization transfer saturation pulse; voxel size = 0.9-mm isotropic.

ARTICLE IN PRESS

- 3D T1 Magnetization Prepared 2 Rapid Acquisition Gradient Echoes (MP2RAGE) sequence with T1 relaxometry map; voxel size = 1-mm isotropic.

MRI analysis

MRI images were processed using the Spinal Toolbox (SCT) version 6.3.[23]

All acquired data were transformed into NIfTI file format and organized using the Brain Imaging Data Structure (BIDS) standard. For all MRI contrasts (T2w, MTon, MToff, DWI, and T1 MP2RAGE), the spinal cord was segmented using the contrast-agnostic model (*sct_deepseg*) [24] to extract a mask for subsequent registration to a template. Vertebral discs were manually labeled on the T2w image, and these labels were used as landmarks for template registration. After virtual straightening of the spine, the T2w image was registered to the PAM50 template using affine and non-rigid registration steps.[25–27] In addition, the MT off image was registered to the MT on image, and the ratio between the two co-registered images ((*MT off – MT on) / MT off*) was calculated for each voxel as the magnetization transfer ratio (MTR, *sct_compute_mtr*). Diffusion processing involved several steps. For each slab, diffusion images were first averaged across the time dimension to obtain a 3D volume; the spinal cord was segmented on the resulting mean diffusion volume. The obtained mask was used for motion correction of the diffusion volume.[28] The diffusion tensor model was fitted, and quantitative maps of fractional anisotropy (FA) and mean diffusivity (MD) were computed (*sct_dmri_compute_dti*). Finally, diffusion slabs were merged, and metrics were extracted in the regions of interest. T1 relaxometry maps, calculated as a default output of the T1 MP2RAGE acquisition, were used to calculate regional T1 longitudinal relaxation times.

First, shape-based analysis was performed on T2-weighted images, in individual space, to compute spinal cord cross-sectional area (CSA) at each slice across the rostro-caudal axis. Next, MTR, diffusion and T1 relaxation metric extractions were conducted in the participant space using the distinct gray matter and white matter probabilistic atlases available in the SCT. Specifically, four regions of interest were selected, including two white matter tracts (ascending and descending tracts) and two gray matter regions (intermediolateral zone, which encompasses the intermediolateral columns, and ventral horns; see supplementary Table S2 for details about the regions). The analysis was restricted to these regions to mitigate the decrease in statistical power due to a relatively small sample size and a large number of variables. Metrics were

ARTICLE IN PRESS

extracted slice-by-slice and averaged across each vertebral level (from C2 to T5), and within each region. For each region, values from the right or left atlas were averaged.

All raw MRI images and processing outputs were visually inspected for quality control.[29]

Statistical analyses

Clinical and demographic data

Statistical analyses were performed using R version 4.3.2 (R Development Core Team, 2023). Continuous data were reported as mean ± standard deviation, and categorical variables as counts and percentages. All tests were two-sided, with significance set at $p < 0.05$ or false discovery rate (FDR)-adjusted $p < 0.05$. Clinical and demographic data were compared across the three groups (HCs, $PD_{RBD(+)}$, and $PD_{RBD(-)}$ patients) using Kruskal-Wallis tests followed by Dunn's post hoc test for multiple comparisons for continuous variables, or Fisher's exact tests for categorical variables.

Group comparisons

Between-group differences in MRI metrics were evaluated using linear models (LMs), with one model per region (ascending tracts, descending tracts, intermediolateral zone, ventral horns) and per MRI metric (CSA, T1, FA, MD, MTR), with 'Group' as the main factor and age and sex as covariates of no interest. Group effects were tested using Type II analysis of variance (ANOVA) F-tests, performed with the 'car' R package (v3.1-2). P-values from the F-tests were corrected for multiple comparisons across regions using FDR correction, with each MRI metric type treated separately. To assess group differences, we tested both two-group and three-group models: the first compared HCs and all PD patients; the second compared HCs, $PD_{RBD(+)}$, and $PD_{RBD(-)}$ patients. For the three-group model, when a significant group effect was detected, post hoc pairwise comparisons were performed using Tukey's method with the 'emmeans' R package (v1.8.9). For each model, assumptions and model fit were checked afterwards by visually inspecting residual distribution plots using the 'ggResidpanel' R package (v0.3.0).

MRI metrics were first averaged across all vertebral levels from C2 to T5 to assess overall spinal cord differences, and then specifically analyzed at the C6–T1 vertebral levels, which correspond to C7-T2 spinal cord segments that

ARTICLE IN PRESS

encompass key centers for cardiovascular autonomic control.[7] Compared to vertebral levels, spinal segments provide a more accurate representation of the spinal cord's functional organization into distinct rootlets.[30,31] Lower levels were excluded due to their higher susceptibility to motion artifacts from cardiac and respiratory activity.

Multivariate analysis

An exploratory multivariate analysis was conducted for illustration purposes to investigate group separation using candidate imaging features preselected from the four spinal cord regions, across all individual vertebral levels (C2 to T5) and for all MRI metrics. Variables were included in the model if the p-value from Kruskal–Wallis tests comparing HCs and PD patients was < 0.15. The discriminative ability of these features was then assessed using partial least squares discriminant analysis (PLS-DA), as implemented in the mixOmics package (v6.26.0). PLS-DA is a supervised machine learning method that enables dimensionality reduction, feature selection, and multiclass classification. The PLS-DA model consists of a small number of orthogonal components, each calculated as a weighted sum of the original imaging variables to maximize covariance with the group labels. The weight values (or loadings) of the resulting components indicate the contribution of each feature to group discrimination across different dimensions. PLS-DA is specifically designed to handle high-dimensional and potentially correlated data in small sample settings.[32]

Model performance was evaluated on the training dataset using a receiver operating characteristic (ROC) analysis with two components, with the area under the ROC curve (AUC) serving as the evaluation metric. Individual-level classification accuracy was determined based on the predicted class assigned to each participant for each component using the maximum distance criterion.

Associations with clinical features

Spearman's rank partial correlation analysis, controlling for age and sex, was performed to investigate relationships between imaging metrics and clinical features at the time of the MRI visit, including disease duration, systolic and diastolic blood pressure drops at 3 minutes, and the cardiovascular subscore of the SCOPA-AUT. P-values were adjusted for multiple correlation tests using the FDR method. Correlations were analyzed across all PD patients as well as within each PD subgroup ($PD_{RBD(+)}$ and $PD_{RBD(-)}$).

ARTICLE IN PRESS

Next, associations between longitudinal changes in systolic and diastolic blood pressure drops (3-min values at 5 years minus baseline) and MRI metrics were assessed using linear regression models, adjusted for age, sex, and baseline blood pressure drops. Associations were reported as standardized regression coefficients (β) with 95% confidence intervals, and p-values from the models were corrected for multiple comparisons across all MRI metric types.

Results

Participants

The final study population included 34 patients with PD and 30 HCs. Following quality check, 8 PD patients were excluded (7 due to insufficient image quality: motion and/or susceptibility artifacts, n=6; severe cervical lordosis, n=1; and 1 due to spinal cord signal abnormalities related to cervical spondylotic myelopathy). Similarly, 8 HCs were excluded (7 due to insufficient image quality: motion and/or susceptibility artifacts, n=5; severe cervical lordosis, n=1; disk protrusion, n=1; and 1 due to spinal cord signal abnormalities). This resulted in 22 HCs and 26 patients with PD, subdivided into $PD_{RBD(+)}$ (n=11) and $PD_{RBD(-)}$ (n=15) subgroups.

There were no significant differences in age or sex distribution between PD patients and HCs, nor within the PD subgroups. As expected, PD patients had higher MDS-UPDRS III ($p<0.0001$) than HCs. RBDSQ scores were significantly higher in the $PD_{RBD(+)}$ subgroup compared to the $PD_{RBD(-)}$ one ($p<0.001$). There were no significant differences between PD subgroups in disease duration, MDS-UPDRS III, SCOPA-AUT scores, cardiovascular SCOPA-AUT subscore, presence of orthostatic hypotension, or systolic and diastolic drops at 3 or 5 minutes (all $p>0.05$), although values tended to be higher in the $PD_{RBD(+)}$ subgroup (Table 1).

Group comparisons

All F-values are reported as $F_{df1,df2}$, where df1 and df2 represent numerator and denominator degrees of freedom. First, our analysis, which covered the spinal cord from C2 to T5 vertebrae, revealed no significant group differences between HCs and all PD patients for any structural MRI metric taken individually. After FDR correction, a trend for higher MTR values in the ventral horn at the cervicothoracic junction (C6-T1)was observed in PD patients compared with HCs, ($F_{1,44}=6.54$, pFDR=0.06; Figure 1, supplementary Table S3). When comparing HCs and the two PD subgroups, this trend remained

ARTICLE IN PRESS

($F_{2,43}$=4.11, pFDR=0.09) with $PD_{RBD(+)}$ patients showing higher MTR values at C6-T1 compared to HCs (pFDR=0.02). No other significant differences were seen after FDR correction for any other MRI metric (Figure 1, supplementary Table S3).

Multivariate analysis

Overall, the PLS-DA model visualization with two components achieved group separation using 26 preselected variables that contributed most to the discrimination (supplementary Table S4).

Component 1 separated $PD_{RBD(-)}$ patients (12/15, 80%, correctly classified) from HCs (17/22, 77.3%) and $PD_{RBD(+)}$ patients (all misclassified as HCs). Component 2 separated HCs (19/22 correctly predicted, 86.4%) from $PD_{RBD(-)}$ (12/15, 80%) and $PD_{RBD(+)}$ (8/11, 72.7%) subgroups. Area under the ROC curve (AUC) values on the training dataset exceeded 0.90 for the discrimination of each group against the others (supplementary Figure S2).

Component 1 was negatively correlated with FA values in the descending tracts (C4, C6, and C7) and with MTR values in the intermediate zone (T3), while showing positive correlations in the descending tracts with T1 relaxation values at C3 and C4, and MD values at C4. Component 2 exhibited negative correlations with MTR values in the ventral horns (C2, C6, and C7) and in the descending tracts (C5 and C6), and positive correlations MD values in the descending tracts (C7) (supplementary Table S5, Figure 2).

ARTICLE IN PRESS

Associations with clinical features

Analyses were performed at the cervicothoracic junction (C6–T1), where group differences showed trends after FDR correction. For the $PD_{RBD(+)}$ subgroup, we found significant positive correlations between systolic drop at 3 minutes and T1 relaxation values in the ascending (ρ =0.78, pFDR=0.03) and descending tracts (ρ =0.81, pFDR=0.03). There were also positive correlations between systolic drop at 3 minutes and MD values in the ascending tracts (ρ =0.77, pFDR=0.04) and ventral horns (ρ =0.75, pFDR=0.04), with a trend in the descending tracts (ρ =0.62, pFDR<0.10) and intermediate zone (ρ =0.64, p<0.10). MD values in the descending tracts were significantly correlated with the cardiovascular subscore of the SCOPA-AUT (ρ =0.75, pFDR=0.04). No significant correlation was found with disease duration, though MD values in the intermediate zone showed a positive trend (ρ =0.62, pFDR<0.10) (Figure 3). No

ARTICLE IN PRESS

significant correlations were observed in the entire PD group, nor in the $PD_{RBD(-)}$ subgroup.

Linear models using MRI metrics and baseline blood pressure drop, and age and sex as covariates in the $PD_{RBD(+)}$ subgroup showed that MD values in the descending (standardized β=0.94, 95% CI [0.42. 1.45], pFDR=0.02) and ascending (standardized β=1.21, 95% CI [0.40, 2.02], pFDR=0.02) tracts were significantly associated with 5-year changes in systolic blood pressure drop. Diastolic changes were also significantly associated with MD values in the ascending (standardized β=1.08, 95% CI [0.37, 1.79], pFDR=0.04), with trends observed for MD (standardized β=0.78, 95% CI [0.11, 1.45], pFDR=0.06) and T1 relaxation (standardized β=0.73, 95% CI [0.17, 1.29], pFDR=0.07) values in the descending tracts (supplementary Table S6). Together, these associations suggest that microstructural alterations in the descending and ascending tracts may be associated with changes in systolic and diastolic blood pressure over time.

Discussion

In this study, we used multimodal MRI to investigate spinal cord involvement in patients with PD in comparison with HCs, and to explore its association cross-sectionally and longitudinally with clinical features of autonomic dysfunction. While group comparisons between PD and HCs, and between PD subgroups, showed no significant differences in MRI metrics, multivariate analysis combining white and gray matter measurements discriminated between PD subgroups and HCs. Within the $PD_{RBD(+)}$ subgroup, we found that blood pressure drops were positively correlated with T1 relaxation and MD values in the ascending and descending tracts, as well as with MD values in the ventral horns and intermediate zone at the cervicothoracic junction, indicating that longer T1 relaxation and MD values were associated with more severe orthostatic hypotension. SCOPA-AUT cardiovascular subscores were positively correlated with MD values in the descending tracts. In addition, longitudinal changes in systolic and diastolic blood pressure drops from baseline to the five-year follow-up were associated with MRI metrics. These findings suggest that subtle microstructural changes in the examined regions may be associated with cardiovascular dysautonomia in PD.

ARTICLE IN PRESS

There is neuropathological evidence showing that PD involves not only the brain but the entire nervous system, including the spinal cord and the peripheral nervous system.[2,8,9] Spinal cord involvement contributes to the occurrence of motor and non-motor symptoms in PD such as autonomic symptoms, constipation, and pain.[3,4] The presence of α-synuclein inclusions has consistently been reported in the thoracic intermediolateral column and the sacral dorsal horns in PD.[2,8,9] In the present study, we did not find statistically significant between-group differences in spinal cord MRI metrics, and we do not provide direct evidence of spinal cord involvement. Nevertheless, in line with our hypothesis, the exploratory associations observed between MRI metrics and clinical features of cardiovascular dysautonomia within the $PD_{RBD(+)}$ subgroup were localized to the cervicothoracic junction, specifically the C6-T1 vertebral levels, corresponding to the C7-T2 spinal segments.[30,31] These spinal segments contain key cardiovascular autonomic centers involved in dysautonomia in PD.[7] This anatomical concordance provides biological plausability for the observed associations, although they should be interpreted cautiously due to the limited sample size and the absence of neuropathological confirmation.

Furthermore, in our study, no correlations were observed in the entire PD group or in the $PD_{RBD(-)}$ subgroup. This lack of association may align with the hypothesis that spinal cord damage is more prominent in $PD_{RBD(+)}$ patients. Indeed, $PD_{RBD(+)}$ patients are expected to follow an ascending model of disease propagation, characterized by earlier and more severe autonomic dysfunction,[10–13] which may mirror why MRI measures in the spinal cord were specifically associated with cardiovascular dysautonomia in this subgroup. Regarding disease propagation, a recent study reported that spinal pathology was only observed in patients already exhibiting Lewy pathology in the brain, with a strong correlation between the amount of spinal cord Lewy pathology and the severity of brain lesions.[9] Using unsupervised K-means analysis, the authors identified two cluster types of spinal and brain Lewy pathology: a caudo-rostral pattern (consistent with an ascending model of disease propagation) and an amygdala-based pattern (i.e, descending model) Lewy pathology types. Interestingly, the spinal cord Lewy pathology type was more strongly associated with the caudo-rostral-based type than the amygdala-based type, further supporting the hypothesis of two distinct propagation patterns of Lewy pathology.[9] While our findings remain exploratory and do not allow to infer about disease progression patterns, larger studies combining spinal cord MRI

ARTICLE IN PRESS

with longitudinal clinical assessments and, where possible, neuropathological data will be needed to validate these observations.

To our knowledge, only one study has investigated spinal cord structural abnormalities at the cervical level (C2-C5) in a cohort of PD patients (n=68), stratified into early (n=23), moderate (n=22) and advanced (n=23) stages, using diffusion, MTR and T2* metrics. Subtle but significant differences were observed between HC and the advanced PD group for FA in the white matter, as well as between HC and the moderate PD group for radial diffusivity in the white matter, based on average values across C2-C5. No significant associations were observed with UPDRS III scores.[33] Unlike our study, the authors did not stratify PD patients based on the presence of absence of RBD and restricted the field of view to the C2-C5 vertebral levels, which might not have captured alterations expected to occur preferentially in the upper thoracic cord and sacral regions.[2,8,9] A resting-state functional MRI (fMRI) study [34] conducted on the same cohort of PD patients as in [35] showed a decrease in functional connectivity in the cervical spinal cord, which was associated with upper limb motor symptoms severity between C4 and C6 spinal levels. However, these functional changes did not correlate with microstructural measures.[35] Similarly, a study on transgenic M83 murine models of PD overexpressing the mutated A53T α-synuclein form (n=22) did not reveal any structural spinal cord abnormalities in comparison with non-transgenic mice (n=13) while oxygen saturation levels in the spinal cord measured with *in vivo* spiral volumetric optoacoustic tomography were shown to be reduced.[36]

Several factors may account for the absence of significant differences in MRI metrics between PD patients and HCs in our study. First, we may have lacked statistical power given the relatively small sample size of PD patients, further reduced after stratification. Second, spinal cord imaging is highly prone to motion artifacts from heart and respiratory activity or swallowing, despite the use of cardiac gating for diffusion imaging, as well as to susceptibility artefacts, particularly affecting the upper thoracic portion. As a result, almost one-quarter (23.3%) of HCs and one-fifth (20.6%) of PD patients were excluded due to insufficient image quality. To minimize the impact of such confounds, conservative quality control criteria were applied to ensure robust and reliable measurements. While these intrinsic technical challenges of imaging the upper thoracic spinal cord currently limit scalability, future technical improvements in

ARTICLE IN PRESS

spinal cord imaging will enable replication of our findings in larger cohorts. Third, the effect size of potential spinal cord alterations was small, with subtle microstructural changes that were hard to capture in PD in comparison with other conditions such as amyotrophic lateral sclerosis [15] or spinal-muscular amyotrophy.[14] Stratifying PD patients based on the presence of orthostatic hypotension would have been interesting. However, the sample size of patients with this feature was too small (5/26).Finally, another limitation was the lack of objective assessment of cardiovascular autonomic function using formal autonomic testing.

To conclude, these preliminary findings suggest possible region-specific associations between structural metrics and cardiovascular dysautonomic features in PD patients with RBD. Correlations at the C6–T1 vertebral levels may support the potential role for cervicothoracic spinal cord alterations in the pathophysiology of autonomic failure in PD despite the lack of significant group-level structural differences. These results require validation and replication in larger study samples to determine whether spinal cord imaging markers can be used as surrogates for autonomic dysfunction in PD. Future studies will include individuals with isolated RBD and incorporate additional measures of cardiovascular function, such as the RR interval. Recent advances in analysis methods, notably rootlet-based instead of vertebral-based analyses,[30,37] might provide more sensitivity to the MRI metrics. Technological advances such as ultra–high-field MRI may improve spatial resolution and signal-to-noise ratio, enabling more sensitive detection of subtle spinal cord changes in PD. Furthermore, resting-state fMRI can reveal network-level alterations, with connectivity changes reflecting PD-related pathology. Combining structural and functional measures may enable the detection of subtle microstructural alterations associated with functional changes, offering a more comprehensive understanding of central nervous systems changes in PD.

ARTICLE IN PRESS

Data Availability Statement

The data obtained in this research are available from the corresponding author upon reasonable request.

Code Availability Statement

The codes used for the analyses are available at https://github.com/sct-pipeline/spine-park.

ARTICLE IN PRESS

ARTICLE IN PRESS

References

1. Braak, H. *et al.* Staging of brain pathology related to sporadic Parkinson's disease. *Neurobiology of Aging* **24**, 197–211 (2003).
2. Del Tredici, K. & Braak, H. Spinal cord lesions in sporadic Parkinson's disease. *Acta Neuropathol* **124**, 643–664 (2012).
3. Postuma, R. B. *et al.* MDS clinical diagnostic criteria for Parkinson's disease. *Mov. Disord.* **30**, 1591–1601 (2015).
4. Schapira, A. H. V., Chaudhuri, K. R. & Jenner, P. Non-motor features of Parkinson disease. *Nat Rev Neurosci* **18**, 435–450 (2017).
5. Rajendran, P. S. *et al.* The vagus nerve in cardiovascular physiology and pathophysiology: from evolutionary insights to clinical medicine. *Semin Cell Dev Biol* **156**, 190–200 (2024).
6. Pyatigorskaya, N. *et al.* Medulla oblongata damage and cardiac autonomic dysfunction in Parkinson disease. *Neurology* **87**, 2540–2545 (2016).
7. Coote, J. H. & Chauhan, R. A. The sympathetic innervation of the heart: Important new insights. *Autonomic Neuroscience* **199**, 17–23 (2016).
8. Tamura, T., Yoshida, M., Hashizume, Y. & Sobue, G. Lewy body-related α-synucleinopathy in the spinal cord of cases with incidental Lewy body disease. *Neuropathology* **32**, 13–22 (2012).
9. Raunio, A. *et al.* Distribution of Lewy-related pathology in the brain, spinal cord, and periphery: the population-based Vantaa 85 + study. *Acta Neuropathol Commun* **10**, 178 (2022).
10. Borghammer, P. & Van Den Berge, N. Brain-First versus Gut-First Parkinson's Disease: A Hypothesis. *J Parkinsons Dis* **9**, S281–S295 (2019).
11. Borghammer, P. *et al.* A postmortem study suggests a revision of the dual-hit hypothesis of Parkinson's disease. *NPJ Parkinsons Dis* **8**, 166 (2022).

ARTICLE IN PRESS

ARTICLE IN PRESS

12. Horsager, J. & Borghammer, P. Brain-first vs. body-first Parkinson's disease: An update on recent evidence. *Parkinsonism & Related Disorders* **122**, 106101 (2024).
13. Passaretti, M. *et al.* Clinical progression and genetic pathways in body-first and brain-first Parkinson's disease. *Molecular Neurodegeneration* **20**, 74 (2025).
14. Querin, G. *et al.* The spinal and cerebral profile of adult spinal-muscular atrophy: A multimodal imaging study. *Neuroimage Clin* **21**, 101618 (2019).
15. Querin, G. *et al.* Spinal cord multi-parametric magnetic resonance imaging for survival prediction in amyotrophic lateral sclerosis. *Eur J Neurol* **24**, 1040–1046 (2017).
16. Cohen-Adad, J. *et al.* Demyelination and degeneration in the injured human spinal cord detected with diffusion and magnetization transfer MRI. *Neuroimage* **55**, 1024–1033 (2011).
17. Seiberlich, N., Gulani, V., Calamante, F. & Campbell-Washburn, A. MRI Biomarkers. in *Advances in Magnetic Resonance Technology and Applications* vol. 1 liii–lxxxvi (Elsevier, 2020).
18. Goetz, C. G. *et al.* Movement Disorder Society-sponsored revision of the Unified Parkinson's Disease Rating Scale (MDS-UPDRS): Scale presentation and clinimetric testing results. *Movement Disorders* **23**, 2129–2170 (2008).
19. Hoehn, M. M. & Yahr, M. D. Parkinsonism: onset, progression and mortality. *Neurology* **17**, 427–442 (1967).
20. Stiasny-Kolster, K. *et al.* The REM sleep behavior disorder screening questionnaire--a new diagnostic instrument. *Mov Disord* **22**, 2386–2393 (2007).

ARTICLE IN PRESS

ARTICLE IN PRESS

21. Visser, M., Marinus, J., Stiggelbout, A. M. & Van Hilten, J. J. Assessment of autonomic dysfunction in Parkinson's disease: the SCOPA-AUT. *Mov Disord* **19**, 1306–1312 (2004).
22. Wieling, W. *et al.* Diagnosis and treatment of orthostatic hypotension. *Lancet Neurol* **21**, 735–746 (2022).
23. De Leener, B. *et al.* SCT: Spinal Cord Toolbox, an open-source software for processing spinal cord MRI data. *NeuroImage* **145**, 24–43 (2017).
24. Bédard, S. *et al.* Towards contrast-agnostic soft segmentation of the spinal cord. *Med Image Anal* **101**, 103473 (2025).
25. De Leener, B. *et al.* PAM50: Unbiased multimodal template of the brainstem and spinal cord aligned with the ICBM152 space. *Neuroimage* **165**, 170–179 (2018).
26. Fonov, V. S. *et al.* Framework for integrated MRI average of the spinal cord white and gray matter: the MNI-Poly-AMU template. *Neuroimage* **102 Pt 2**, 817–827 (2014).
27. Lévy, S. *et al.* White matter atlas of the human spinal cord with estimation of partial volume effect. *Neuroimage* **119**, 262–271 (2015).
28. Xu, J. *et al.* Improved in vivo diffusion tensor imaging of human cervical spinal cord. *Neuroimage* **67**, 64–76 (2013).
29. Valošek, J. & Cohen-Adad, J. Reproducible Spinal Cord Quantitative MRI Analysis with the Spinal Cord Toolbox. *Magnetic Resonance in Medical Sciences* **23**, 307–315 (2024).
30. Valošek, J., Mathieu, T., Schlienger, R., Kowalczyk, O. S. & Cohen-Adad, J. Automatic segmentation of the spinal cord nerve rootlets. *Imaging Neurosci (Camb)* **2**, imag–2–00218 (2024).

ARTICLE IN PRESS

ARTICLE IN PRESS

31. Frostell, A., Hakim, R., Thelin, E. P., Mattsson, P. & Svensson, M. A Review of the Segmental Diameter of the Healthy Human Spinal Cord. *Front Neurol* **7**, 238 (2016).
32. Boulesteix, A.-L. & Strimmer, K. Partial least squares: a versatile tool for the analysis of high-dimensional genomic data. *Brief Bioinform* **8**, 32–44 (2007).
33. St-Onge, S. *et al.* Parkinson's disease in the spinal cord: An exploratory study to establish T2*w, MTR and diffusion-weighted imaging metric values. *Imaging Neuroscience* **3**, IMAG.a.1015 (2025).
34. Landelle, C. *et al.* Altered Spinal Cord Functional Connectivity Associated with Parkinson's Disease Progression. *Movement Disorders* **38**, 636–645 (2023).
35. St-Onge, S. *et al.* Parkinson's disease in the spinal cord: an exploratory study to establish T2*w, MTR and diffusion-weighted imaging metric values. *NeuroLibre Reproducible Preprints* 39 (2025) doi:10.55458/neurolibre.00039.
36. Combes, B. F. *et al.* Spiral volumetric optoacoustic tomography of reduced oxygen saturation in the spinal cord of M83 mouse model of Parkinson's disease. *Eur J Nucl Med Mol Imaging* **52**, 427–443 (2025).
37. Bédard, S. & Cohen-Adad, J. Automatic measure and normalization of spinal cord cross-sectional area using the pontomedullary junction. *Front Neuroimaging* **1**, 1031253 (2022).

ARTICLE IN PRESS

ARTICLE IN PRESS

ARTICLE IN PRESS

ARTICLE IN PRESS

Author contributions

L.C. designed and conceptualized the study, collected and analyzed the data, drafted the manuscript for intellectual content.

F.X.L conceptualized the study, analyzed the data, and revised the manuscript for intellectual content.

J.C.A., M.G.P., J.N., J.V., K.W., analyzed the data and revised the manuscript.

C.L., J.D., and A.D., helped with the methodology and revised the manuscript for intellectual content.

E.B., C.J., N.P., S.S. G.M., J.C.C, I.A. collected the data, and revised the manuscript for intellectual content.

M.V. and S.L. designed and conceptualized the study, collected the data, and revised the manuscript for intellectual content.

ARTICLE IN PRESS

ARTICLE IN PRESS

Declaration of Competing Interests

Nothing related to this work.

J.C.C. has served in advisory boards for Alzprotect, Bayer, Ferrer, iRegene, Servier, UCB, Roche, and received grants from AXA and the ICM Foundation outside of this work.

Funding/Acknowledgments

The study was funded by grants from Agence Nationale de la Recherche (ANRMNP 2009, Nucleipark), DHOS-Inserm (2010, Nucleipark), France Parkinson, École des NeuroSciences de Paris (ENP), Fondation pour la Recherche Médicale (FRM), and the Investissements d'Avenir, IAIHU-06 (Paris Institute of Neurosciences – IHU), ANR-11-INBS-0006, Fondation d'Entreprise EDF, Biogen Inc., Fondation Thérèse and René Planiol, Unrestricted support for Research on Parkinson's disease from Energipole and Société Française de Médecine Esthétique.

L.C. received funding from the Société Française de Radiologie (SFR), the Collège des Enseignants en Radiologie de France (CERF), and the Société Française de Neuroradiologie (SFNR).

J.V. received funding from the European Union's Horizon Europe research and innovation program under the Marie Skłodowska-Curie grant (no. 101107932).

E.B. received fellowship funding from Association France Parkinson, Biogen Inc., and the European Union's Horizon Europe research and innovation program under the Marie Skłodowska-Curie Actions (no. 101066055, acronym HERMES).

ARTICLE IN PRESS

Figures

Figure 1: MTR values across vertebral levels in HCs and PD patients

Mean values with shaded areas representing the 95% confidence intervals of Locally Estimated Scatterplot Smoothing (LOESS)-smoothed MTR values (y-axis) across vertebral levels (x-axis) for different regions of interest are shown for HCs, all PD patients, and PD subgroups. The gray shaded rectangle indicates the C6–T1 junction, where group differences in average MRI values were assessed using an F-test adjusted for age and sex.

ARTICLE IN PRESS

Abbreviations: HC, healthy controls; VH, ventral horns; IZ, intermediate zone; MTR, magnetization transfer ratio; PD; Parkinson's disease; $PD_{RBD(+)}$, PD with RBD; $PD_{RBD(-)}$, PD without RBD; RBD, Rapid-Eye Movement Sleep Behavior Disorder.

Figure 2: Multivariate analysis

Individual (left) and variable (right) plots illustrate the two-component PLS-DA model based on 26 preselected FA, MD, MTR, and T1 relaxation variables across vertebral levels from C2 to T5. The individual plot shows fair separation among the groups of HCs, $PD_{RBD(+)}$, and $PD_{RBD(-)}$. Percentages on the axes represent the variance explained by each component. Colors in the variable plot correspond to variable types: FA (red), MD (blue), MTR (green), and T1 relaxation (purple).

Abbreviations: HC, healthy controls; VH: ventral horns; IZ, intermediate zone; MTR, magnetization transfer ratio; PD; Parkinson's disease; $PD_{RBD(+)}$, PD with RBD; $PD_{RBD(-)}$, PD without RBD ; RBD, Rapid-Eye Movement Sleep Behavior Disorder.

ARTICLE IN PRESS

Figure 3: Associations between clinical variables and MRI measurements at the cervicothoracic junction of the spinal cord in the $PD_{RBD(+)}$ subgroup

(A, C) Spearman's rank partial correlation matrices (rho coefficients) between clinical variables and averaged T1 relaxation (A) and MD (C) values across the C6-T1 vertebral levels in the $PD_{RBD(+)}$ subgroup. Asterisks indicate correlations that were significant before correction for multiple comparisons, while symbols in parentheses indicate those that remain significant after FDR correction. Circles specifically denote non-significant trends ($p < 0.10$). Significance levels are indicated as follows: $p < 0.10$ (°), $p < 0.05$ (*), $p < 0.01$ (**), and $p < 0.001$ (***). (B, D) Scatterplots with linear regression lines showing significant correlations (after FDR correction) between systolic blood pressure drop values at 3 minutes (adjusted for age and sex) and T1 relaxation values in the descending tracts (B), as well as MD values in the ascending tracts (D), also adjusted for age and sex, in the $PD_{RBD(+)}$ subgroup. These correlations were not significant in the $PD_{RBD(-)}$ subgroup. The shaded area around each regression

ARTICLE IN PRESS

line represents the 95% confidence interval of the fitted model. Marginal density plots along the top and right margins illustrate the distributions of systolic blood pressure drops at 3 minutes, T1 relaxation values in the descending tracts (B), and MD values in the ascending tracts (D) for each subgroup, respectively. Raw Spearman's rho coefficients and p-values without correction are indicated on each plot.

Abbreviations: FDR, false discovery rate; MD, mean diffusivity; PD; Parkinson's disease; $PD_{RBD(+)}$, PD with RBD; RBD, Rapid-Eye Movement Sleep Behavior Disorder; SCOPA-AUT, SCales for Outcomes in PArkinson's disease - Autonomic Dysfunction; T1, longitudinal relaxation time.

ARTICLE IN PRESS

ARTICLE IN PRESS

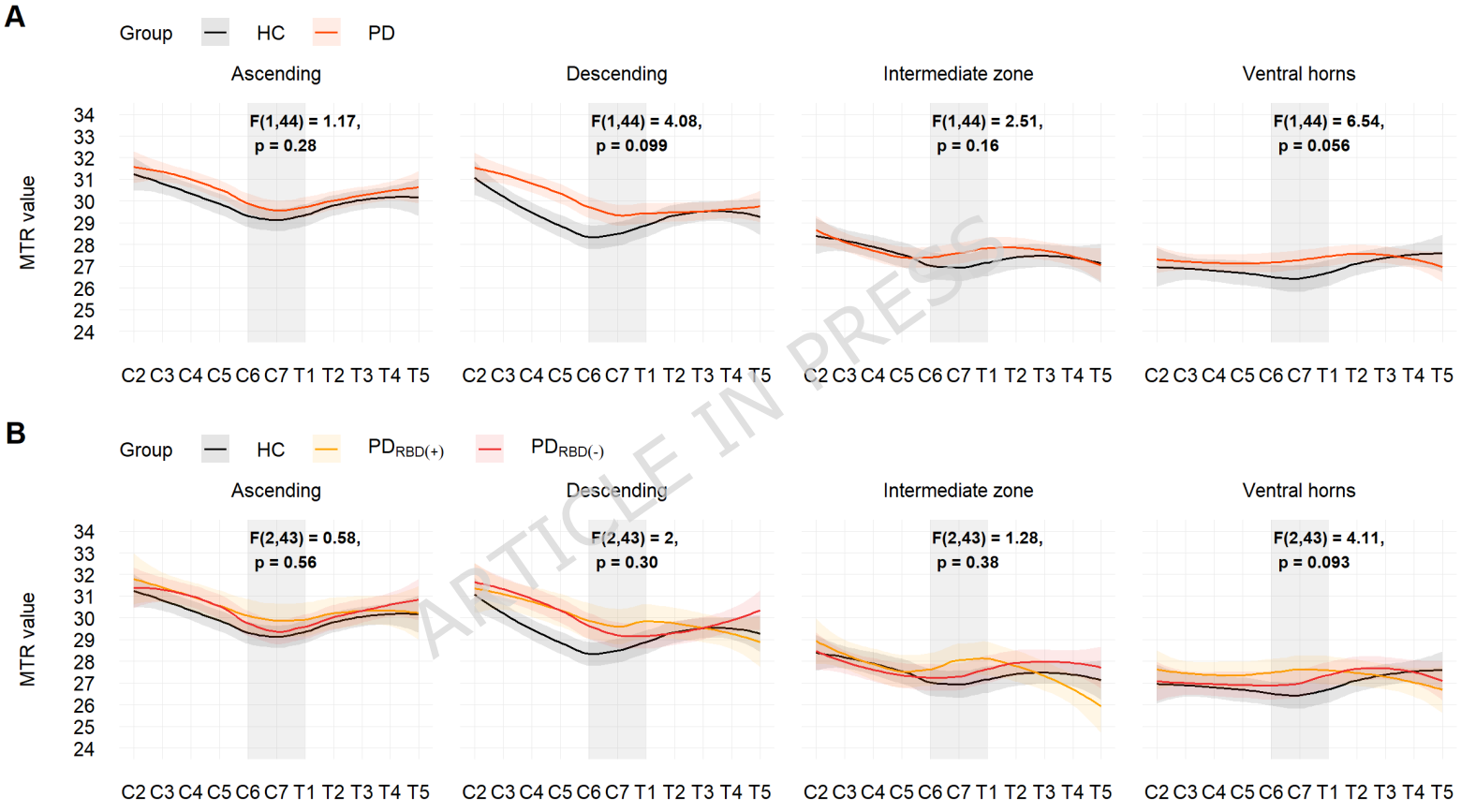

ARTICLE IN PRESS

ARTICLE IN PRESS

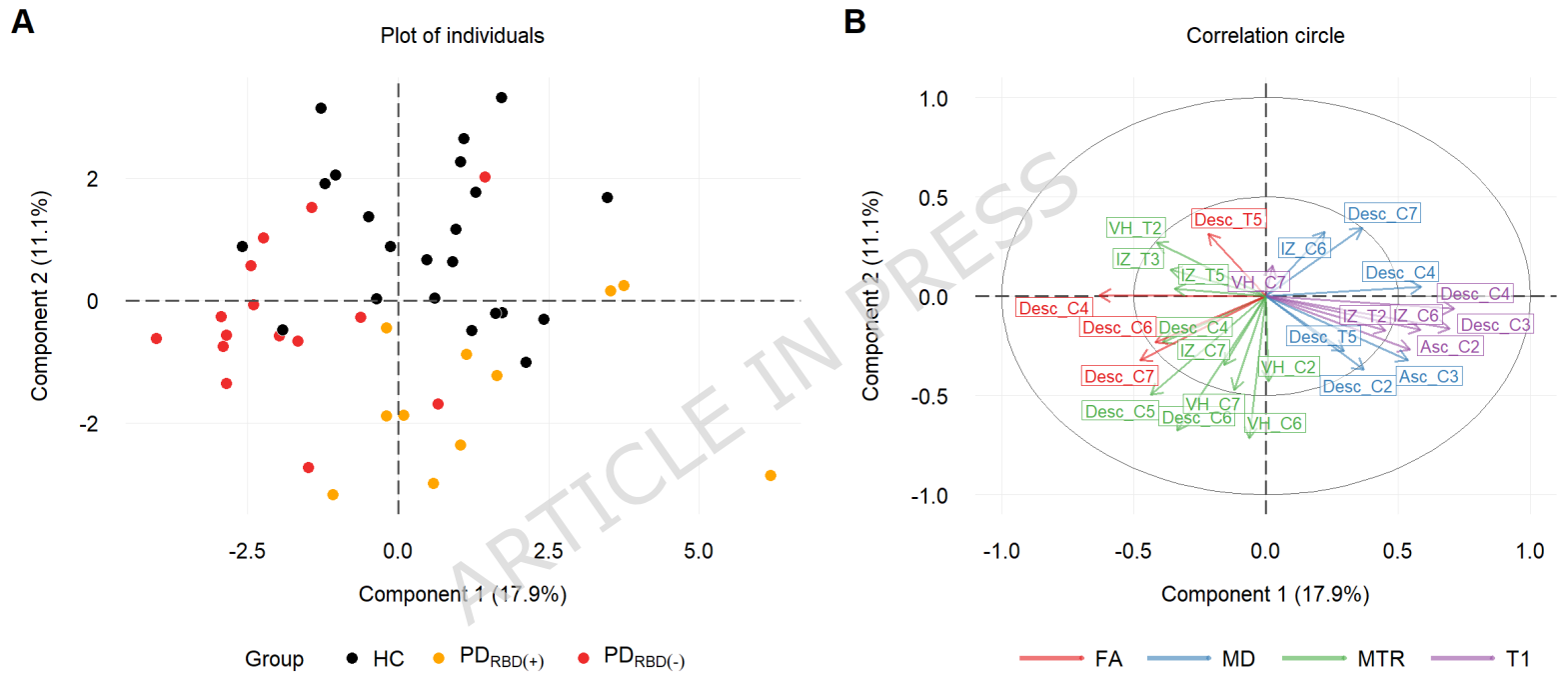

ARTICLE IN PRESS

ARTICLE IN PRESS

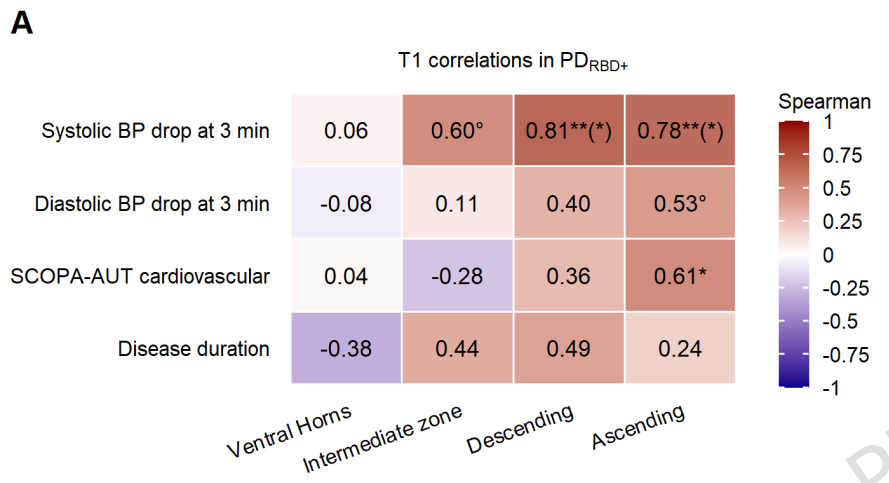

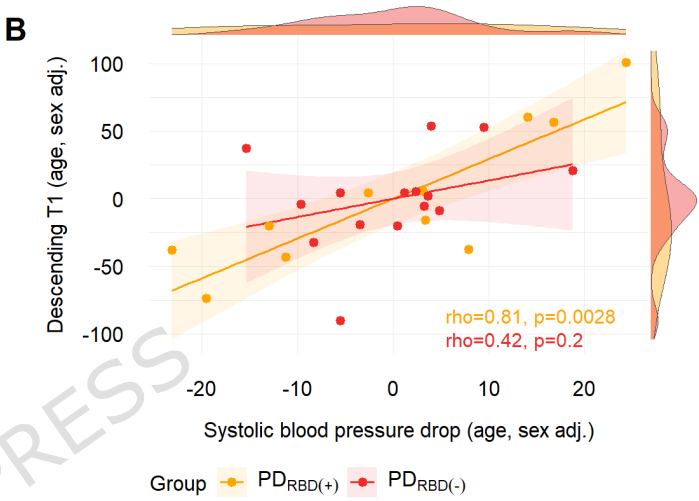

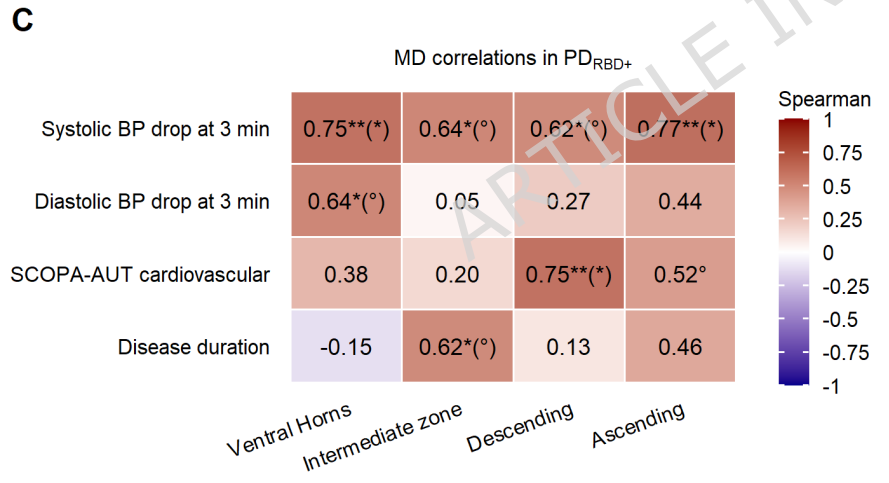

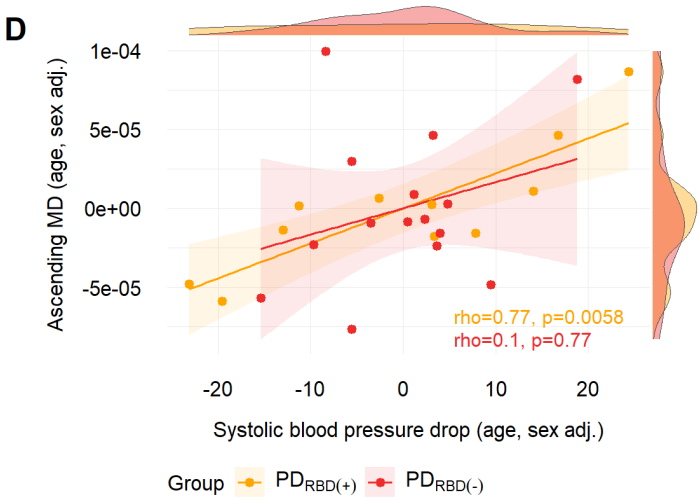

ARTICLE IN PRESS

ARTICLE IN PRESS

Table 1: Participants' demographical and clinical characteristics

	HC	PD			Global tests	Post hoc tests
		All PD	*$PD_{RBD(+)}$*	*$PD_{RBD(-)}$*		
n	22	26	11	15	---	---
Age (years)	67.9 ± 8.7 [53-83]	68.2 ± 9.0 [47-82]	71.4 ± 9.4 [47-82]	65.8 ± 8.3 [53-78]	0.21	ns
Sex (female), n (%)	13 (59.1%)	15 (57.7%)	7 (63.6%)	8 (53.3%)	0.87	ns
Disease duration (months)	---	45.7 ± 13.9 [20.2-80.5]	47.6 ± 16.9 [20.2-80.5]	44.2 ± 11.7 [21.7-61.1]	0.57	ns
MDS-UPDRS III (off)	4.1 ± 3.3 [0-10]	28.6 ± 11.5 [9-67]	32.1 ± 14.1 [14-67]	26.0 ± 8.8 [9-39]	**<0.0001**	$PD_{RBD(+)}$>HC***, $PD_{RBD(-)}$>HC***
Hoehn and Yahr scale	---	1.8 ± 0.6 [1-3]	2.0 ± 0.4 [1-3]	1.6 ± 0.6 [1-3]	ns	ns
RBDSQ	7.75 ± 3.79 [2-14]	18.19 ± 18.21 [0-74]	32.6 ± 19.4 [12-74]	7.8 ± 6.6 [0-17]	**<0.0001**	$PD_{RBD(+)}$>HC**, $PD_{RBD(+)}$>$PD_{RBD(-)}$**
Orthostatic hypotension	1 (8.3%)	5 (19.2%)	4 (36.4%)	1 (6.7%)	0.12	ns
Systolic blood pressure drop at 3min (mmHg)	0.8 ± 8.9 [-12-13]	3.3 ± 12.1 [-20-33]	4.8 ± 16.1 [-20-33]	2.2 ± 8.5 [-13-23]	0.64	ns
at 5min (mmHg)	2.2 ± 11.1 [-19-25]	3.2 ± 13.9 [-25-35]	4.3 ± 18.6 [-25-35]	2.47 ± 9.8 [-15-22]	0.88	ns
Diastolic blood pressure drop at 3min (mmHg)	2.9 ± 8.7 [-22-7]	-0.8 ± 7.0 [-11-13]	1.2 ± 7.6 [-10-13]	-2.2 ± 6.4 [-11-9]	0.46	ns
at 5min (mmHg)	-4.3 ± 6.4 [-16-7]	0.4 ± 7.5 [-13-21]	3.2 ± 7.6 [-5-21]	-1.7 ± 6.9 [-13-10]	0.07	ns
SCOPA-AUT	8.9 ± 7.0 [1-25]	15.0 ± 6.9 [3-26]	16.7 ± 7.2 [4-25]	13.7 ± 6.6 [3-26]	**<0.001**	$PD_{RBD(+)}$>HC*, $PD_{RBD(-)}$>HC
SCOPA cardiovascular subscore	0.3 ± 0.5 [0-1]	0.7 ± 0.9 [0-3]	1.0 ± 1.1 [0-3]	0.4 ± 0.5 [0-1]	0.15	ns
MoCA	27.3 ± 2.47 [22-30]	27.5 ± 2.0 [24-30]	27.7 ± 2.1 [24-30]	27.3 ± 2.0 [24-30]	0.770	ns

ARTICLE IN PRESS

ARTICLE IN PRESS

Quantitative variables are summarized as mean ± standard deviation [min-max] and categorical variables as counts and percentages. Clinical data other than the MDS-UPDRS III were only available in 12 HCs. Statistically significant effects for global comparisons with Kruskal-Wallis or Fisher's exact tests are shown in bold. Asterisks indicate the significance level of the post hoc comparisons: adjusted $p < 0.05$ (*), adjusted $p < 0.01$ (**), adjusted $p < 0.001$ (***).

Abbreviations: F: female; HC, healthy controls; M: male; MDS-UPDRS part III, Movement Disorder Society Unified Parkinson's Disease Rating Scale part III; ns, non-significant; PD; Parkinson's disease; $PD_{RBD(+)}$, PD with RBD; $PD_{RBD(-)}$, PD without RBD; RBDSQ, REM Sleep Behavior Disorder Screening Questionnaire; RBD, Rapid-Eye Movement Sleep Disorder; SCOPA-AUT SCales for Outcomes in PArkinson's disease - Autonomic Dysfunction.

ARTICLE IN PRESS